Research on α-Mangostin Nanoformulations for Anti-Ovarian Cancer

Journal:	*Materials Lab*
Manuscript ID	MATLAB-2025-0003.R1
Manuscript Type:	Original Article
Date Submitted by the Author:	12-Mar-2025
Complete List of Authors:	Liu, Xia; Sichuan University, Department of Pharmacy Zhang, Zhenyu; Sichuan University, Department of Plastic Liu, Jie; Sichuan University Gao, Xiang; Sichuan University Wang, Bilan; Sichuan University, Department of Pharmacy
Keywords:	Alpha-mangostin, apoptosis, hydrogel, ovarian cancer, proliferation
Speciality:	Others

Dear editors and reviewers:

Thank you for your letter and for the reviewers' comments concerning our manuscript entitled "**Research on α-Mangostin Nanoformulations for Anti-Ovarian Cancer** " (***manuscript number:MATLAB-2025-0003***).Those comments are all valuable and very helpful for revising and improving our paper, as well as the important guiding significance to our researches. The reviewers' comments are presented in blue, while our responses are shown in black. Additionally, the specific revisions incorporated into the updated manuscript are highlighted in yellow.

We have studied comments carefully and have made correction which we hope meet with approval.

Reviewer: This work evaluated the effects of intraperitoneally administered α-mangostin nanoparticles in an ovarian cancer mouse model. More importantly, this work developed a hydrogel-encapsulated α-mangostin nanoparticle drug delivery system, which enhanced the water solubility and bioavailability of pure α-mangostin, demonstrating potential clinical applications in ovarian cancer treatment. Some specific comments are listed as follows:

Main comments:

1. What are the storage conditions for α-mangostin in the animal experiments?

Response 1: Thank you very much for your comments and suggestions. We fully agree that the introduction of the storage conditions for α-Mangostin in animal experiments is very important. We will add the storage conditions of α-Mangostin related formulations in animal experiments to the manuscript.

We store α-Mangostin related formulations at a low temperature of 4°C. Considering that the reagent is administered in vivo, it is necessary to provide a low-temperature environment to inhibit the growth and reproduction of microorganisms and ensure the purity and quality of the reagent. Secondly, α-Mangostin nanoformulations are prone to decomposition and deterioration at room temperature, and a low-temperature environment can slow down the rate of deterioration. Lastly, α-Mangostin nano-thermogel is in a solid state at room temperature

and cannot be injected in vivo. A low-temperature environment is required to turn it into an injectable liquid formulation. Therefore, the low-temperature environment of 4°C provides a relatively stable and safe condition for the storage of α-Mangostin related formulations, which helps to extend the shelf life of the reagent and maintain its quality and performance.

2. In the cytotoxicity experiments, the cytotoxicity of mPEG-PCL against ID8 cells should be provided.

Response 2: Thank you very much for your comments and suggestions. We fully agree that it is crucial to supplement the cytotoxicity of mPEG-PCL against ovarian cancer ID8 cells to demonstrate the in vivo antitumor efficacy of α-Mangostin nanoformulations. This key information has now been incorporated into the revised manuscript (Figure 2.a).

ID8 cells in the logarithmic growth phase were seeded into a 96-well plate and allowed to grow overnight. Subsequently, the cells were treated with mPEG-PCL at appropriate concentration gradients (50, 25, 12.5, 6.25, 3.125, 1.56, 0.78, 0.39, 0.195, 0.0975, 0 μg/mL) and cultured for 24 hours. Then, 20 μL of MTT solution was added and incubated in the dark at 37°C for 1 hour. The solution in the 96-well plate was then discarded, and 150 μL of DMSO solution was added. The absorbance at 490 nm for each well was measured using a microplate reader, confirming that mPEG-PCL has no significant cytotoxic effect on ovarian cancer ID8 cells.

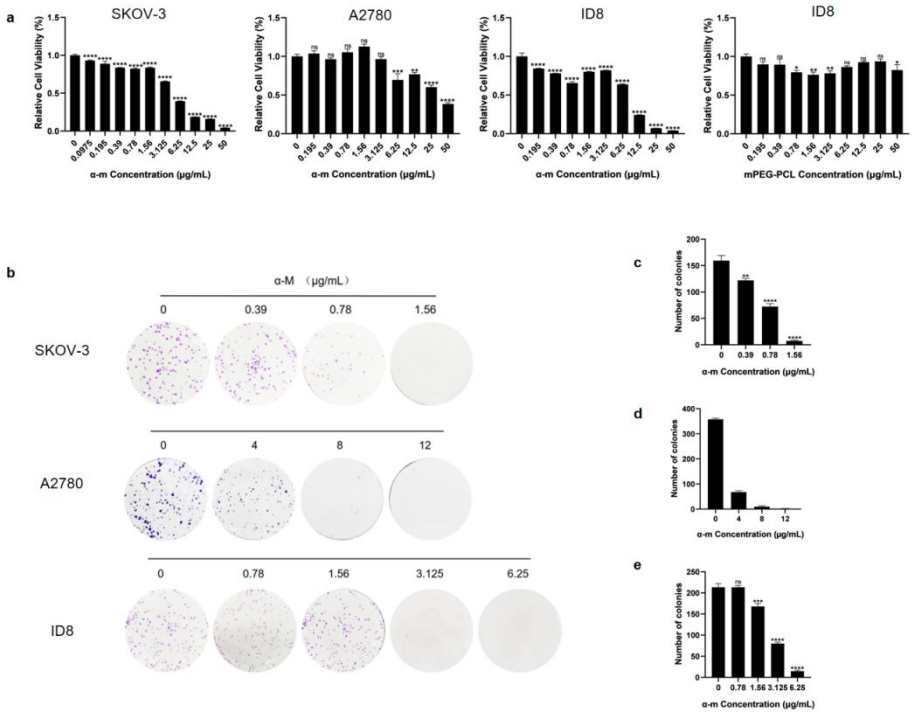

Cell viability studies and proliferation inhibition effects of alpha-mangostin. a. After co-incubating different concentrations of alpha-mangostin nanoformulations with ovarian cancer cells SKOV-3, A2780, and ID8 for 24 or 48 hours in vitro, cell viability was assessed using the MTT assay kit (n=3). After co-incubating ovarian cancer cells ID8 with various concentrations of mPEG-PCL for 24 hours in vitro, cell viability was assessed using the MTT assay kit (n=3). b. Two weeks after co-incubating different concentrations of alpha-mangostin nanoformulations with ovarian cancer cells SKOV-3, A2780, and ID8 in vitro, colony formation of cells in different treatment groups (n=3). c. Count of clones formed by SKOV-3 cells after treatment with different concentrations of alpha-mangostin nanoformulations for two weeks. d. Count of clones formed by A2780 cells after treatment with different concentrations of alpha-mangostin nanoformulations for two weeks. e. Count of clones formed by ID8 cells after treatment with different concentrations of alpha-mangostin nanoformulations for two weeks.

3. In Figure 5, the process of α-mangostin nanoparticles and F127 forming a thermosensitive gel should be described.

Response 3: Thank you very much for your comments and suggestions, and we apologize for initially omitting the data on the thermosensitive transition process of the F127 hydrogel. This

key information has now been incorporated into the revised manuscript (Figure 1.e).

The higher the concentration of the hydrogel, the lower its solidification temperature; conversely, the higher its melting temperature. At 4°C, the 20% hydrogel exhibits fluidity; at 26°C, the 20% F127 hydrogel is in a solid state. This is consistent with the state of the nanoformulation shown in Figure 1.d, demonstrating that the F127 hydrogel is in a solid state in the animal body, allowing for the sustained release of the drug.

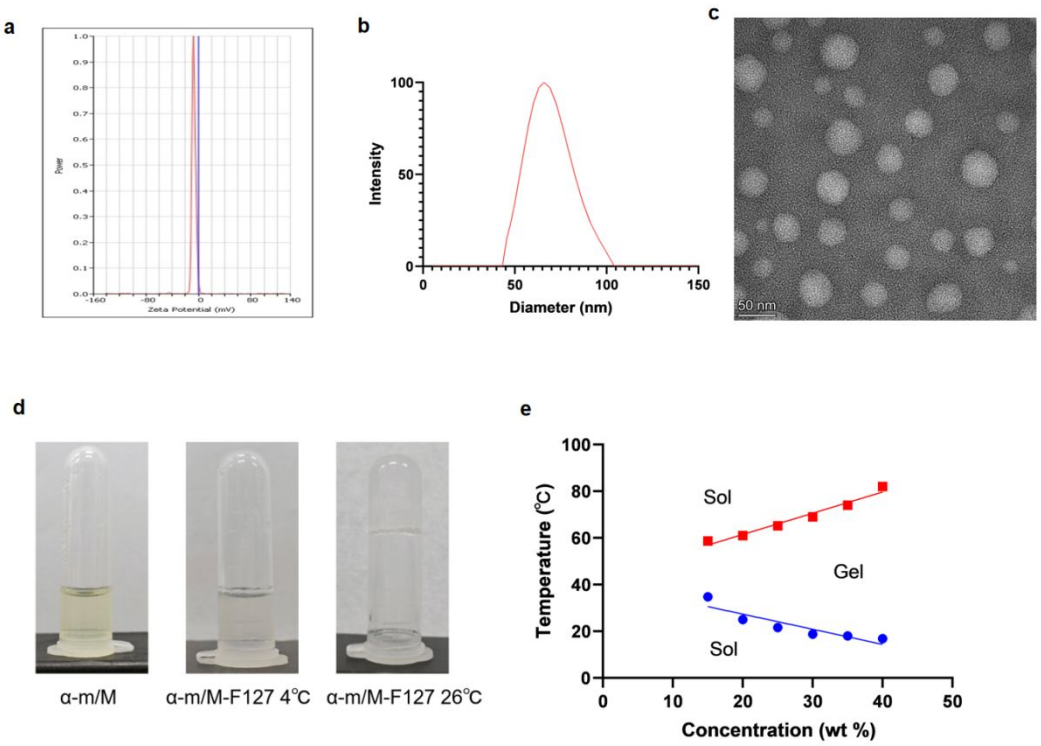

Characterization of alpha-mangostin nanoformulations. a. The zeta potential graph of the alpha-mangostin nanoformulation. b. The particle size distribution graph of the alpha-mangostin nanoformulation. c. The transmission electron microscopy (TEM) image of the alpha-mangostin nanoformulation. d. The schematic diagram of the alpha-mangostin nanoformulation. e. The process of F127 forming a thermosensitive gel.

4. The language and grammar of this work should be further polished to a native level.

Response 4: Thank you for your valuable feedback on the language and grammar of our manuscript. We fully agree that clear and precise communication is essential for the dissemination of scientific research. To address this concern, we have conducted a thorough review of the manuscript ourselves, paying close attention to sentence structure, terminology, and overall

coherence. We have made numerous revisions to improve readability and ensure that the language is both precise and accessible to a broad scientific audience. We have also shared the manuscript with colleagues who are native English speakers and experts in our field. Their feedback has been invaluable in identifying and correcting any remaining language issues, further enhancing the quality of our manuscript. We are confident that these efforts have significantly improved the language and grammar of our manuscript, making it more polished and professional. We have highlighted the revised sections in the manuscript in yellow for your reference.

Manuscript Submission Template

- **Title page**

Research on α-Mangostin Nanoformulations for Anti-Ovarian Cancer

- **Author list**

Xia Liu[1,#], Zhenyu Zhang[2,#], Jie Liu[3*], Xiang Gao[3*], Bilan Wang[1*]

[1]Department of Pharmacy,West China Second University Hospital of Sichuan, National Key Laboratory of Biotherapy, Sichuan University, Sichuan 610000, China

[2]Department of Plastic and Burn Surgery, West China School of Medicine, West China Hospital, Sichuan University, Chengdu, 610041, China.

[3]National Key Laboratory of Biotherapy, Sichuan University, Sichuan 610000, China.

[#]These authors made equal contributions to this work.

* Corresponding author: Jie Liu, Xiang Gao and Bilan Wang

E-mail: liujie2011@scu.edu.cn, xianggao@scu.edu.cn and bilan@scu.edu.cn

Academic Press

- **Abstract**

Ovarian cancer is a type of malignant tumor with a high incidence rate, poor prognosis, and a tendency to relapse. There is a lack of effective therapeutic drugs in the treatment process of ovarian cancer. Alpha-mangostin, an oxyanthenone-type compound, has anti-tumor biological activities. Compared with traditional chemotherapeutic drugs, the advantage of natural source chemotherapeutic drugs lies in lower toxicity, killing tumor cells while reducing damage to normal cells, alleviating the adverse reactions and multi-drug resistance caused by chemotherapy. The nanoformulation was prepared using the thin-film dispersion method, with a particle size of approximately 60 nm. Compared to other drug formulations, its advantage lies in its good biocompatibility. Hydrogels are excellent drug carriers, possessing temperature sensitivity that enables controlled drug release. In this study, the water gel was used as a carrier to wrap the alpha-mangostin nanoparticles to form a nanocomposite hydrogel, and its effects on ovarian cancer cells were evaluated comprehensively, including cell proliferation, apoptosis, and cytotoxicity. Research has confirmed that alpha-mangostin nano-hydrogels can induce apoptosis and inhibit cell proliferation, showing good therapeutic effects on ovarian cancer cells. In summary, alpha-mangostin hydrogel has the potential to become a novel drug formulation for the treatment of ovarian cancer.

- **Keywords**

Alpha-mangostin, apoptosis, hydrogel, ovarian cancer, proliferation

- **Main text**

1. Introduction

Ovarian cancer is one of the three deadliest gynecological malignancies, [1–3] accounting for 3.1% of cancer deaths in China. It is a type of malignant tumor in the female reproductive system that is typically detected late and has a poor prognosis. While immunotherapy is rapidly developing, surgery and chemotherapy remain the primary treatments for ovarian cancer. [4–7] The commonly used chemotherapeutic drugs for ovarian cancer include paclitaxel and platinum-based drugs. [8] However, during chemotherapy, these drugs can cause severe toxic side effects on the human body, [9–14] ultimately leading to suboptimal treatment outcomes for the tumor. This has prompted us to develop new chemotherapeutic drugs that reduce the toxic side effects of chemotherapy on the human body, in order to achieve better therapeutic effects.

Given the high toxicity and other drawbacks of traditional chemotherapeutic drugs, we have turned our attention to natural compounds. Alpha-mangostin is a xanthone compound isolated from the pericarp of the mangosteen fruit. [15,16] Compared to traditional chemotherapeutic drugs, alpha-mangostin has lower toxicity. In addition to its antibacterial and anti-inflammatory activities, it can also induce apoptosis and regulate cellular signaling pathways, showing antitumor activity in cancers such as breast cancer, [17] liver cancer, [18] and ovarian cancer. It is a highly promising candidate for chemotherapy. Compared to traditional chemotherapeutic drugs, alpha-Mangostin exhibits higher safety. However, the naturally occurring alpha-Mangostin is limited in its bioavailability due to its poor water solubility and rapid metabolism. Therefore, improving the water solubility of the drug is an excellent way to enhance its therapeutic effects. [19–21] Nanomedicines have the advantages of increasing drug solubility, extending blood circulation, targeting tumors, controlled drug release, and low toxic side effects , showing great potential in cancer treatment. [22,23]

As nanotechnology continues to advance, nanoscale materials have increasingly become a cornerstone in enhancing drug delivery and optimizing therapeutic outcomes. By formulating alpha-mangostin into nanoparticles, such as those encapsulated by mPEG-PCL polymers, it is hoped to overcome the issue of poor drug solubility. However, the problem of rapid drug metabolism at the tumor site still persists. Therefore, by preparing a biodegradable sustained-release drug delivery system, that is, encapsulating alpha-mangostin nanoparticles with hydrogel, the distribution of drugs at

the local tumor site is enhanced, and systemic toxic side effects are reduced, thereby enhancing the efficacy of chemotherapeutic drugs. Currently, hydrogels used for cancer treatment on the market include F127, PEG hydrogels, and hyaluronic acid hydrogels, among others. Ovarian cancer is a peritoneal tumor, and F127, with its good biocompatibility and temperature responsiveness, has demonstrated a sustained-release effect in the peritoneal cavity, making it an excellent carrier in the treatment of ovarian cancer. Local treatment with hydrogel is expected to overcome common problems in chemotherapy, such as low solubility and rapid drug metabolism, allowing for reduced dosage and frequency of administration, and increasing the effective local drug concentration in tumors, [24,25] which greatly improves the space for drug toxicity and water solubility issues.

Based on the aforementioned findings and building on previous research, we have designed a nanoformulation drug delivery system for alpha-mangostin to address drug dispersion issues, and then encapsulated it within a biodegradable hydrogel to achieve sustained drug release to achieve the goal of reducing toxicity and enhancing efficacy. This drug delivery system is expected to become a new method for chemotherapy treatment of ovarian cancer.

2. Materials and methods

2.1. Materials

Alpha-mangostin, 3-(4,5-dimethylthiazol-2-yl)-2,5-diphenyltetrazolium bromide (MTT) was purchased from Sigma-Aldrich (St. Louis, MO, USA), the Annexin V-FITC/PI apoptosis detection kit was acquired from BD Biosciences (Franklin Lake, NJ, USA). The dead-end fluorescent TUNEL system was provided by Promega (Madison, WI, USA). Hematoxylin and eosin (H&E) were purchased from Shanghai Baoteng Company, China. CD31 antibody (ab28364) and Ki67 antibody (ab15580) were acquired from Abcam (MA, US). Transmission electron microscopy was provided by the Ceshigo (Sichuan, China) scientific research service platform.

C57BL/6 mice were purchased from Huafukang (Beijing, China). The mice, aged 6 to 8 weeks and female, were housed under specific pathogen-free (SPF) conditions.

2.2. Methods

2.2.1. Preparation and Characterization of Alpha-mangostin Nanoformulation Hydrogel

Weighed separately, mPEG-PCL was dissolved in dichloromethane solution, and alpha-mangostin was dissolved in anhydrous ethanol. The two were thoroughly mixed, water-bath evaporated, and then dried under vacuum to form a film. Then, distilled water was added to hydrate the film, and it was squeezed through a filter.

The particle size and zeta potential of the alpha-mangostin nanoparticles were determined using a particle size analyzer, and their morphology was observed using a transmission electron microscope. The state of the alpha-mangostin nanoparticles combined with the hydrogel was observed using a test tube flip method at different temperatures.

2.2.2. Cell Culture

Ovarian cancer cells A2780 and SKOV-3 are cultured in DMEM medium containing 100 ml/L fetal bovine serum, 10 μg/mL penicillin, and 10 μg/mL streptomycin; ID8 cells are cultured in 1640 medium containing 100 ml/L fetal bovine serum, 10 μg/mL penicillin, and 10 μg/mL streptomycin. All cell culture processes are carried out in an incubator at 37℃ with 5% carbon dioxide.

2.2.3. Cell Viability Assay

The MTT assay is used to detect cellular proliferation vitality and to determine the IC50 values of alpha-mangostin on A2780 cells, SKOV-3 cells, and ID8 cells. Cells in the logarithmic growth phase are taken, digested with trypsin, collected, and resuspended. The cells are then seeded in a 96-well plate at a density of 7000 cells per well with 100 μL per well and allowed to grow overnight. Subsequently, alpha-mangostin at appropriate concentration gradients is added and the cells are cultured for 24 h and 48 h. Then, 20 μL of MTT is added and incubated in the dark at 37℃ for 1 hour. After discarding the solution in the 96-well plate, 150 μL of DMSO solution is added to dissolve the formazan product. The absorbance of each well at 490 nm is detected using a microplate reader to determine the IC50 values of alpha-mangostin for each ovarian cancer cell line. ID8 cells in the logarithmic growth phase were seeded into a 96-well plate using the same method. After overnight growth, the cells were treated with mPEG-

Academic Press

PCL at appropriate concentration gradients and cultured for 24 and 48 hours, respectively. Subsequently, 20 μL of MTT solution was added and incubated in the dark at 37° C for 1 hour. The solution in the 96-well plate was then discarded, and 150 μL of DMSO solution was added. The absorbance at 490 nm for each well was measured using a microplate reader to verify the cytotoxic effects of mPEG-PCL on ID8 cells.

2.2.4. Apoptosis Assay

SKOV-3 cells were treated with alpha-mangostin at concentrations of 0, 1.56, 3.125, 6.25, and 12.5 μg/mL; similar treatments were applied to A2780 and ID8 cells, with A2780 cells being treated at concentrations of 0, 6, 8, 10, 12, 14, and 16 μg/mL. ID8 cells were treated at concentrations of 0, 0.78, 1.56, 3.125, 6.25, and 12.5 μg/mL. All cells were incubated in the culture medium for 24 hours, after which the cells were collected and prepared into single-cell suspensions. The single-cell suspensions were then stained using the Annexin V-FITC/PI kit, and subsequently, flow cytometry was used to analyze the stained cells.

2.2.5. Cell Cycle Analysis

Seed the SKOV-3 cell suspension at an appropriate density in a 6-well plate and culture overnight. Treat SKOV-3 cells with alpha-mangostin at concentrations of 0, 1.56, 3.125, 6.25, and 12.5 μg/mL; treat A2780 cells with alpha-mangostin at concentrations of 0, 4, 6, 8, and 10 μg/mL; treat ID8 cells with alpha-mangostin at concentrations of 0, 1.56, 3.125, 6.25, and 12.5 μg/mL. After 24 hours of drug exposure, collect the cells in flow cytometry tubes, centrifuge at 1500 r for 3 minutes, and wash with pre-chilled phosphate-buffered saline (PBS) before fixing in 75% ethanol at 4°C for more than 12 hours. Stain the cells with a PI (propidium iodide) staining solution containing RNase, and analyze the cells using the ACEA NovoCyteTM flow cytometer (Novo Express International, Inc., USA) at the lowest speed.

2.2.6. Cell Proliferation Analysis

Prepare a cell suspension of SKOV-3 cells in the logarithmic growth phase, and seed the cells in a 12-well plate at a density of 600 cells per well, then culture overnight. Treat SKOV-3 cells with alpha-mangostin at concentrations of 0, 0.39, 0.78, and 1.56 μg/mL; treat A2780 cells with alpha-mangostin at concentrations of 0, 4, 8, and 12

μg/mL; treat ID8 cells with alpha-mangostin at concentrations of 0, 0.78, 1.56, 3.125, and 6.25 μg/mL. After 24 hours of treatment, replace the culture medium and incubate in an incubator at 37°C with 5% carbon dioxide, changing the medium every three days. When the cells form visible colonies in the culture plate, stain the cells with 0.1% crystal violet.

2.2.7. Western Blot Detection of Related Proteins

Take logarithmic growth phase ovarian cancer cells A2780, SKOV-3, and ID8, digest them with trypsin, and gently pipette to prepare a single-cell suspension. Seed the cell suspension at an appropriate density in a six-well plate, and then place it in a carbon dioxide incubator for static culture. After the cells adhere, treat the cells with alpha-mangostin at different concentrations, and extract proteins with 1×SDS at 24 h and 48 h later; place the protein samples in a 100℃ metal bath and boil for 10-15 min.

Use a 12.5% SDS-PAGE gel to separate the proteins, activate a 0.45 μm PVDF membrane with methanol, and transfer in an ice water bath for 0.5-1.5 hours; block with 5% TBST milk for 1 hour, then wash with TBST and incubate with the primary antibody at 4°C overnight; the next day, wash the strips with TBST on a shaker for 5 min; subsequently, incubate with the horseradish peroxidase (HRP)-conjugated secondary antibody for 1 hour; wash the strips with TBST on a shaker for 6×5 min; soak the strips in the developing solution, expose, and observe the strips, repeating the experiment three times.

2.2.8. In Vivo Antitumor Study

Establish a C57BL/6 ovarian cancer model with ID8 cells transfected with luciferase (ID8-luc). Culture ID8-luc cells in a 10 cm culture dish until confluent, digest with 0.25% trypsin, centrifuge at 1500 r for 3 minutes to obtain a cell pellet, resuspend in 1640 medium without serum, and continue centrifugation. Resuspend the ID8-luc cell pellet in 1640 medium without serum and inoculate the C57BL/6 mice intraperitoneally with approximately 1×10^7 cells per mouse. After three weeks of tumor growth, randomly divide the mice into five equal groups. Administer intraperitoneal injections every three days at a dose of 500 μL per mouse, and measure mouse weight before each administration. On the day after the last administration, inject 100 μL of 15 mg/mL luciferin substrate intraperitoneally, anesthetize the mice with isoflurane, and assess

tumor size using the IVIS in vivo imaging system. All drugs were stored in a refrigerator at 4°C.

For C57BL/6 mice after 40 days of administration, collect samples by removing one eyeball with forceps, place the eyeball blood in a 1.5 mL Eppendorf tube, and store in a 4℃ refrigerator overnight. Centrifuge at 3000 r for 15 minutes, take the supernatant, and store in a -80℃ refrigerator for future use. After blood collection, euthanize the mice, record the volume of ascites, fix the limbs on a dissection board, open the abdominal cavity, remove the tumor and viscera, weigh the tumor, and fix it in 4% paraformaldehyde solution for future use.

2.2.9. Immunofluorescence

After fixing the tumors in paraformaldehyde, they were embedded in paraffin, sectioned, and then stained with the One-step TUNEL In Apoptosis Kit. The number of apoptotic tumor cells in tumor tissues from different groups of mice was compared under a fluorescence microscope, and the image results were processed using OlyVIA software.

2.2.10. Immunohistochemistry

Tumors fixed in paraformaldehyde were embedded in paraffin, sectioned, and stained with H&E and IHC. Mouse tumor tissues from each experimental group were harvested and stored at -80°C. The tumor tissues were then processed into frozen sections, and immunohistochemical staining for mouse CD31 and Ki67 was performed on the frozen sections from each group to compare the differences in vascular density and tumor cell proliferation activity in the tumor tissues of the mice. Slides were scanned using the Olympus fully automatic pathology imaging and analysis system VS200, and the image results were processed using OlyVIA software.

2.2.11. Drug Safety Assessment

When evaluating the efficacy of drugs in vivo, monitor the changes in mouse body weight simultaneously, observing the weight changes in both the treatment and control groups; collect the hearts, livers, spleens, lungs, and kidneys from mice treated with the drug for hematoxylin-eosin (H&E) staining to observe any pathological changes in these major organs after drug treatment; collect serum from mice treated with nanomedicine for biochemical analysis. Collect the supernatant serum from the venous ~~blood of mice and use an automated biochemical analyzer to measure the indicators in~~

the serum, further assessing whether the nanomedicine has any side effects such as liver and kidney function damage.

2.2.12. Statistical Analysis

Statistical analysis is performed using GraphPad Prism 9.0 software, with ordinary one-way ANOVA. All statistical values are represented as the mean ± standard error of the mean (SEM) of three independent samples.

A value of $p < 0.05$ is considered significant (*$p < 0.05$, **$p < 0.01$, ***$p < 0.001$, ****$p < 0.0001$), indicating a statistically significant difference; a value of $P > 0.05$ is considered not significant (ns), indicating no statistically significant difference.

3. Results

3.1. Material characterization

After dissolving alpha-mangostin and mPEG-PCL separately, self-assembly was used to encapsulate alpha-mangostin with mPEG-PCL to form nano-micelles, which were then incorporated into a hydrogel to create alpha-mangostin nano-composite hydrogels. Characterization was performed using a particle size analyzer, transmission electron microscopy (TEM), and the tube inversion method. Dynamic Light Scattering (DLS) spectroscopy determined the size distribution and zeta potential of the micelles. The α-m/M micelles were spherical with an average diameter of 58.15 nm (Figure 1.a), and the zeta potential results indicated that the micelle surface was negatively charged, with a zeta potential of -7.54 mV (Figure 1.b). TEM observations of the morphology of α-m/M revealed a spherical structure with an average diameter of about 45 nm (Figure 1.c), which was consistent with the results obtained from DSL. The tube inversion method showed that the alpha-mangostin nano-micelles had flowability, and when alpha-mangostin nanomicelles were encapsulated with a 20% F127 hydrogel carrier, the system remained fluid at 4°C, but solidified at 26°C (Figure 1.d), with the temperature-dependent transition process illustrated in Figure 1.e.

3.2. Alpha-mangostin induces the inhibition of proliferation in ovarian cancer cells.

The cytotoxicity of alpha-mangostin was studied through MTT assays. The MTT results showed that after treating ovarian cancer cell lines A2780, SKOV-3, and ID8 ~~with various concentrations of alpha-mangostin (50, 25, 12.5, 6.25, 3.125, 1.56, 0.78,~~

0.39, 0.195, 0.0975, 0 μg/mL) for 24 hours, the survival rates of the treatment groups with 50, 25, 12.5, 6.25, and 3.125 μg/mL significantly decreased compared to the control group ($P < 0.05$); similar results were observed after treating A2780, SKOV-3, and ID8 cells for 48 hours (Figure 2.a). The data above indicate that alpha-mangostin has an inhibitory effect on the proliferation of ovarian cancer cells A2780, SKOV-3, and ID8 in vitro. Additionally, ID8 ovarian cancer cells were treated with mPEG-PCL at various concentrations (50, 25, 12.5, 6.25, 3.125, 1.56, 0.78, 0.39, 0.195, 0.0975, 0 μ g/mL) for 24 hours. Compared to the control group, there was no significant change in cell viability in any of the treatment groups ($P > 0.05$) (Figure 2a). The results of the clonogenic assay further confirmed the inhibitory effect of alpha-mangostin on the proliferation of ovarian cancer cells (Figure 2.b), and the inhibitory effect is positively correlated with the drug concentration.

By analyzing the impact of alpha-mangostin on the cell cycle using flow cytometry, the results showed that in A2780 cells, as the drug concentration increased, tumor cells were arrested in the G_0/G_1 phase (Figure 3.a), and similar results were observed in the ID8 and SKOV-3 cell lines. Cyclin D1 is an important regulatory molecule of the cell cycle. Western blot analysis revealed that the expression levels of proteins including cyclin D1 and CDK4 decreased with increasing drug concentration (Figure 3.c), indicating that alpha-mangostin downregulates cyclin D1 and CDK4 proteins. Therefore, it can be preliminarily inferred that alpha-mangostin arrests cells in the G_0/G_1 phase through this pathway, which is consistent with the results of flow cytometry and suggests that alpha-mangostin inhibits the proliferation of ovarian cancer cells.

Nevertheless, the precise mechanism underlying the antiproliferative effects of α-mangostin on tumor cells remains to be elucidated. Preliminary speculation based on literature review suggests that its proliferative inhibition effect is achieved by blocking the AKT and STAT3 pathways and activating the mAPK pathway. Western blot analysis confirmed that in A2780 cells, the expression of phosphorylated AKT and STAT3 proteins decreased with increasing drug concentration (Figure 3.c), while the expression of phosphorylated mAPK proteins increased. The same effect was observed in SKOV-3 and ID8 cells. Thus, the antiproliferative effects of α-mangostin may stem from its ability to inhibit phosphorylation pathways like AKT and STAT3, while activating others such as mAPK.

3.3. Observing the effect of alpha-mangostin on ovarian cancer cell apoptosis using the Annexin V-FITC/PI double staining method.

As shown in Figure 4.a, treating the A2780 cell line with different concentrations of alpha-mangostin (0, 6, 8, 10, 12 μg/mL) for 24 hours resulted in apoptosis rates of 2.99%, 30.55%, 60.69%, 74.65%, and 77.25%, respectively. Compared to the control group, all treatment groups showed significant differences ($P < 0.05$), and similar effects were observed in SKOV-3 and ID8 cells. The results indicate that alpha-mangostin can induce apoptosis in ovarian cancer cells, and the apoptotic effect is enhanced with increasing drug concentration. Further confirmation of alpha-mangostin's ability to induce cell apoptosis was provided by western blot analysis of apoptosis-related proteins such as caspase-3, Cleaved caspase-3, caspase-8, Cleaved caspase-8, caspase-9, Cleaved caspase-9, Bcl-2, and Bax (Figure 4.c). The Bcl-2 protein family regulates apoptosis, and the results show that alpha-mangostin upregulates Bax protein and downregulates Bcl-2 protein, activating the caspase cascade reaction, further confirming that alpha-mangostin can induce cell apoptosis, which is consistent with the results of flow cytometry.

3.4. In vivo antitumor efficacy and safety evaluation of alpha-mangostin

To assess the effectiveness of alpha-mangostin nanoformulations in inhibiting tumor growth in vivo, we established an ID8-luc peritoneal tumor model and administered intraperitoneal injections 14 times with glucose solution (GS), hydrogel (F127), naked alpha-mangostin (α-m), alpha-mangostin micelles (α-m/M), and hydrogel-encapsulated alpha-mangostin micelles (α-m/M-F127) at 3-day intervals. The alpha-mangostin nanoformulation was synthesized through self-assembly (Figure 5. a), and F127 was used to encapsulate the alpha-mangostin nanoformulation (Figure 5.b) for intraperitoneal administration. After the completion of the drug administration, the mice were euthanized, and peritoneal tumors were extracted. It was observed that compared to the control group, α-m, α-m/M, and α-m/M-F127 all exhibited inhibitory effects on tumor growth. The treatment with alpha-mangostin micelles showed better therapeutic effects than the naked alpha-mangostin, and the hydrogel-encapsulated alpha-mangostin micelles in the treatment group showed the best efficacy (Figure 5.c), with the smallest tumor weight (Figure 5.e). Moreover, there was no significant difference in mouse body weight compared to the control group (Figure 5.f). In vivo

Academic Press

imaging results also demonstrated that the hydrogel-encapsulated alpha-mangostin micelles had the best inhibitory effect on tumor cells (Figure 5.d).

To explore the in vivo antineoplastic mechanisms of hydrogel-encapsulated alpha-mangostin nanoformulations, sections of ID8 peritoneal tumors were stained with CD31, Ki67, and TUNEL, as shown in Figure 6.a. In the GS and F127 groups, tumors were observed to have an abundance of blood vessels with a positive rate as high as 30%. Compared to the micelle group and the naked drug group, the number of blood vessels was slightly reduced, with a positive rate of about 10%, but both were higher than in the treatment group. At the same time, the treatment group had the highest TUNEL positive rate, followed by the micelle group. The results indicate that hydrogel-encapsulated alpha-mangostin nanoformulations can effectively inhibit tumor angiogenesis and tumor cell proliferation, and control tumor development in vivo by inducing apoptosis.

Sections of the heart, liver, spleen, lungs, and kidneys fixed in paraformaldehyde were stained with H&E (Figure 7), and the morphology of the organs was observed, with no significant pathological changes found in the main organs.

Mouse blood samples collected were placed in a Cobas C311 automatic analyzer for blood biochemical analysis, and the serum analysis results showed that all indicators were within the normal range, with no significant differences between groups(Figure 8).

4. Discussion

Currently, the primary therapeutic approaches for ovarian cancer are surgery and chemotherapy. However, due to the significant toxic side effects of conventional chemotherapeutic drugs, poor prognosis is often encountered in the treatment of ovarian cancer. [1,26,27] This has become a major limiting factor in the treatment process, reducing the efficacy of chemotherapeutic drugs and potentially leading to tumor recurrence and metastasis. Alpha-mangostin, as a natural compound, has garnered attention for its potential antitumor activity, [28] and studies suggest that it may combat toxic side effects in ovarian cancer treatment, offering a new approach. However, alpha-mangostin is hydrophobic, which reduces its bioavailability in the body. To address these issues, we prepared alpha-mangostin into a nanoformulation using the thin-film dispersion method, thereby enhancing its solubility in water [29–31] and improving

bioavailability. The nanoformulation improves the drug's dispersion in biological systems, allowing for a more consistent and effective delivery to the tumor site. To further delay drug release, we encapsulated alpha-mangostin nanoformulations within a hydrogel, which, as a biocompatible carrier, forms a gel in vivo and continuously releases the entrapped drug, achieving the purpose of sustained drug release. [32–35] Compared to traditional chemotherapeutic drugs, the hydrogel-encapsulated alpha-mangostin nanoformulation system has a significant antitumor effect. By encapsulating alpha-mangostin into nanocomplexes and employing hydrogel as a carrier, we not only enhance its solubility in the body but also achieve sustained drug release. This novel drug delivery system is expected to play an important role in the future treatment of ovarian cancer.

Through in vitro experiments, we have demonstrated that alpha-mangostin exhibits superior antitumor efficacy compared to conventional chemotherapeutic agents, with its effects being positively correlated with drug concentration. Utilizing the MTT assay, we have not only preliminarily established the cytotoxic impact of alpha-mangostin on ovarian cancer cells but also ascertained that mPEG-PCL exerts no significant cytotoxicity on ID8 ovarian cancer cells. It is documented that alpha-mangostin has multiple mechanisms of cancer suppression. Studies have found that AKT and STAT3 proteins are overactivated in many tumors, and alpha-mangostin can block the phosphorylation signal transduction pathways of AKT and STAT3, thereby inhibiting cell proliferation. In addition, alpha-mangostin can activate the mAPK/p-mAPK signaling pathway that regulates apoptosis, promoting the phosphorylation and activation of mAPK protein, and inducing apoptosis in tumor cells. Not only that, but alpha-mangostin can also upregulate the expression of the pro-apoptotic protein Bax and promote the cleavage of caspase-3 protein, thereby promoting cell apoptosis. [36–39] Furthermore, we have found that alpha-mangostin can reduce the expression of cyclin D1, CDK4, and other cycle-related proteins, causing tumor cells to arrest at specific phases of the cell cycle, halting the progression of the cell cycle, and thus inhibiting the proliferation of tumor cells. [40] In summary, alpha-mangostin exerts its antitumor effects through various mechanisms, including inhibiting the proliferation of tumor cells, promoting apoptosis in tumor cells, and blocking the progression of the tumor cell cycle.

It has been demonstrated through in vivo experiments that alpha-mangostin exhibits reduced toxicity compared to conventional chemotherapeutic agents. In vitro

Academic Press

experiments have preliminarily confirmed the cytotoxicity of alpha-mangostin to ovarian cancer cells through MTT assays. Clonogenic assay data showed that alpha-mangostin can inhibit the proliferation of ovarian cancer cells. Analysis of the cell cycle progression by flow cytometry revealed that alpha-mangostin can arrest ovarian cancer cells in the G_0/G_1 phase. Further investigation with western blot experiments confirmed that alpha-mangostin arrests the cell cycle in the G_0/G_1 phase by downregulating cyclin D1 and CDK4. mAPK protein is phosphorylated and activated under apoptotic stimuli, thereby promoting apoptosis and inhibiting tumor growth. STAT3 is often over-phosphorylated and activated in cancer, and when the phosphorylation pathways of AKT and STAT3 are inhibited, the proliferative behavior of tumor cells is also suppressed. Therefore, its mechanisms of proliferation inhibition and apoptosis induction may function through the inhibition of AKT and STAT3 phosphorylation and the activation of mAPK phosphorylation pathways. By detecting cell apoptosis with flow cytometry, we found that alpha-mangostin can significantly promote apoptosis in ovarian cancer cells, and this promotional effect is positively correlated with drug concentration. To assess the impact of alpha-mangostin on apoptosis-related signaling pathways, the drug was applied to ovarian cancer cells, and the expression of apoptotic proteins was detected by western blot. Our results support the hypothesis that alpha-mangostin promotes cell apoptosis through the Bax/Bcl-2 pathway and activates the caspase-3, caspase-8, and caspase-9 cascade to initiate apoptosis, which is consistent with the conclusions of flow cytometry.

A hydrogel was utilized through in vivo experiments to encapsulate alpha-mangostin nanoformulations, enhancing the solubility and improving the therapeutic efficacy of the drug. Following treatment with the alpha-mangostin nanoformulation hydrogel, the rate of tumor growth was significantly slowed, and the formation of ascites was effectively reduced, ameliorating the poor prognosis. Observations of tumor tissue sections after staining revealed that the alpha-mangostin nanoformulations could markedly inhibit tumor angiogenesis and suppress the proliferation of tumor cells, thereby limiting tumor growth. Encouragingly, no significant pathological changes were observed in the major organs of mice treated with this method. Throughout the experiment, we closely monitored the body weight changes of the mice, and the results showed no significant difference in weight between the treatment group and the control group, nor were there any weight fluctuations or deaths due to drug toxicity. All blood biochemical indicators were within the normal range, further confirming the safety of the alpha-mangostin nanoformulations. In summary, the hydrogel-encapsulated alpha-

mangostin nanoformulations demonstrated significant antitumor effects in in vivo experiments, with good safety and tolerability, providing strong experimental evidence for their potential as a treatment for ovarian cancer. Future research will further explore the optimal dosage, frequency of administration, and the potential for combination with other therapeutic methods for this formulation.

5. Conclusions

In summary, we have successfully constructed a novel drug delivery system of hydrogel-encapsulated alpha-mangostin nanoformulations and conducted an in-depth exploration of their potential mechanisms in inhibiting ovarian cancer cells. In vitro experiments revealed that alpha-mangostin plays a role in inhibiting proliferation and promoting apoptosis in ovarian cancer cells. In in vivo experiments, we utilized animal models to assess the antitumor effects of the hydrogel-encapsulated alpha-mangostin nanoformulations and found that the formulation not only effectively inhibits tumor angiogenesis but also significantly suppresses tumor cell proliferation, thereby limiting tumor growth. And compared to traditional chemotherapy drugs, this drug system shows lower toxicity. Therefore, we believe that the hydrogel-encapsulated alpha-mangostin nanoformulations have the potential to become a new chemotherapeutic agent for the treatment of ovarian cancer. Future research will focus on further optimizing the formulation's recipe, dosage, and administration regimen, as well as conducting broader preclinical and clinical studies to verify their efficacy and safety in the treatment of ovarian cancer.

6. Acknowledgments

This work was supported by the National Natural Science Foundation of China (32371545, China), the Sichuan Science and Technology Program (No. 2025ZNSFSC0545 and 2023NSFSC1931, China)

7. Conflict of interest

The authors declare no conflict of interest.

8. Author contributions

Xia Liu and Zhengyu Zhang concuted the research, analyzed the data, and wrote the paper;Jie Liu, Bilan Wang and Xiang Gao made revisions to the article; all authors had approved the final version.

9. References

[1] KONSTANTINOPOULOS P A, MATULONIS U A. Clinical and translational advances in ovarian cancer therapy[J]. Nature Cancer, 2023, 4(9): 1239-1257.

[2] EISENHAUER E A. Real-world evidence in the treatment of ovarian cancer[J]. Annals of Oncology: Official Journal of the European Society for Medical Oncology, 2017, 28(suppl_8): viii61-viii65.

[3] ARMSTRONG D K, ALVAREZ R D, BAKKUM-GAMEZ J N, et, al. Ovarian Cancer, Version 2.2020, NCCN Clinical Practice Guidelines in Oncology[J]. Journal of the National Comprehensive Cancer Network: JNCCN, 2021, 19(2): 191-226.

[4] KUROKI L, GUNTUPALLI S R. Treatment of epithelial ovarian cancer[J]. BMJ (Clinical research ed.), 2020, 371: m3773.

[5] VAN STEIN R M, AALBERS A G J, SONKE G S, et, al. Hyperthermic Intraperitoneal Chemotherapy for Ovarian and Colorectal Cancer: A Review[J]. JAMA oncology, 2021, 7(8): 1231-1238.

[6] GHISONI E, MOROTTI M, SARIVALASIS A, et, al. Immunotherapy for ovarian cancer: towards a tailored immunophenotype-based approach[J]. Nature Reviews. Clinical Oncology, 2024, 21(11): 801-817.

[7] GARBUZENKO O B, SAPIEZYNSKI J, GIRDA E, et, al. Personalized Versus Precision Nanomedicine for Treatment of Ovarian Cancer[J]. Small (Weinheim an Der Bergstrasse, Germany), 2024, 20(41): e2307462.

[8] RICHARDSON D L, ESKANDER R N, O'MALLEY D M. Advances in Ovarian Cancer Care and Unmet Treatment Needs for Patients With Platinum Resistance: A Narrative Review[J]. JAMA oncology, 2023, 9(6): 851-859.

[9] KOPECKA J, TROUILLAS P, GAŠPAROVIĆ A Č, et, al. Phospholipids and cholesterol: Inducers of cancer multidrug resistance and therapeutic targets[J]. Drug Resistance Updates: Reviews and Commentaries in Antimicrobial and Anticancer Chemotherapy, 2020, 49: 100670.

[10] GAO Q, FENG J, LIU W, et, al. Opportunities and challenges for co-delivery nanomedicines based on combination of phytochemicals with chemotherapeutic drugs in cancer treatment[J]. Advanced Drug Delivery Reviews, 2022, 188: 114445.

[11] SATHASIVAM T, KAI J, SUGIARTO S, et, al. Nano-Strategies for Lignin Biomaterials toward Cancer Therapy[J]. Advanced Healthcare Materials, 2023, 12(19): e2300024.

[12] LIANG Y, LIU Z Y, WANG P Y, et, al. Nanoplatform-based natural products co-delivery system to surmount cancer multidrug-resistant[J]. Journal of Controlled Release: Official Journal of the Controlled Release Society, 2021, 336: 396-409.

[13] WANG L, WANG X, ZHU X, et, al. Drug resistance in ovarian cancer: from mechanism to clinical trial[J]. Molecular Cancer, 2024, 23(1): 66.
[14] FREYER D R, BROCK P R, CHANG K W, et, al. Prevention of cisplatin-induced ototoxicity in children and adolescents with cancer: a clinical practice guideline[J]. The Lancet. Child & Adolescent Health, 2020, 4(2): 141-150.
[15] NAUMAN M C, JOHNSON J J. The purple mangosteen (Garcinia mangostana): Defining the anticancer potential of selected xanthones[J]. Pharmacological Research, 2022, 175: 106032.
[16] AIZAT W M, AHMAD-HASHIM F H, SYED JAAFAR S N. Valorization of mangosteen, “The Queen of Fruits,” and new advances in postharvest and in food and engineering applications: A review[J]. Journal of Advanced Research, 2019, 20: 61-70.
[17] RAY-COQUARD I, PAUTIER P, PIGNATA S, et, al. Olaparib plus Bevacizumab as First-Line Maintenance in Ovarian Cancer[J]. The New England Journal of Medicine, 2019, 381(25): 2416-2428.
[18] MOHAMED G A, AL-ABD A M, EL-HALAWANY A M, et, al. New xanthones and cytotoxic constituents from Garcinia mangostana fruit hulls against human hepatocellular, breast, and colorectal cancer cell lines[J]. Journal of Ethnopharmacology, 2017, 198: 302-312.
[19] GUTIERREZ A M, FRAZAR E M, X KLAUS M V, et, al. Hydrogels and Hydrogel Nanocomposites: Enhancing Healthcare through Human and Environmental Treatment[J]. Advanced Healthcare Materials, 2022, 11(7): e2101820.
[20] MIKHAIL A S, MORHARD R, MAUDA-HAVAKUK M, et, al. Hydrogel drug delivery systems for minimally invasive local immunotherapy of cancer[J]. Advanced Drug Delivery Reviews, 2023, 202: 115083.
[21] LIU R, LIANG Q, LUO J Q, et, al. Ferritin-Based Nanocomposite Hydrogel Promotes Tumor Penetration and Enhances Cancer Chemoimmunotherapy[J]. Advanced Science (Weinheim, Baden-Wurttemberg, Germany), 2024, 11(3): e2305217.
[22] HAN Y, WEN P, LI J, et, al. Targeted nanomedicine in cisplatin-based cancer therapeutics[J]. Journal of Controlled Release, 2022, 345: 709-720.
[23] MOORE K N, OZA A M, COLOMBO N, et, al. Phase III, randomized trial of mirvetuximab soravtansine versus chemotherapy in patients with platinum-resistant ovarian cancer: primary analysis of FORWARD I[J]. Annals of Oncology: Official Journal of the European Society for Medical Oncology, 2021, 32(6): 757-765.
[24] ASHRAFIZADEH M, ZARRABI A, BIGHAM A, et, al. (Nano)platforms in breast cancer therapy: Drug/gene delivery, advanced nanocarriers and immunotherapy[J]. Medicinal Research Reviews, 2023, 43(6): 2115-2176.

[25] HUA Y, YIN H, LIU X, et, al. Salt-Inducible Kinase 2-Triggered Release of Its Inhibitor from Hydrogel to Suppress Ovarian Cancer Metastasis[J]. Advanced Science (Weinheim, Baden-Wurttemberg, Germany), 2022, 9(22): e2202260.
[26] SESSA C, SCHNEIDER D T, PLANCHAMP F, et, al. ESGO-SIOPE guidelines for the management of adolescents and young adults with non-epithelial ovarian cancers[J]. The Lancet. Oncology, 2020, 21(7): e360-e368.
[27] O'MALLEY D M. New Therapies for Ovarian Cancer[J]. Journal of the National Comprehensive Cancer Network: JNCCN, 2019, 17(5.5): 619-621.
[28] ZHANG S, ZHANG Y, WANG W, et, al. A combination strategy of DOX and VEGFR-2 targeted inhibitor based on nanomicelle for enhancing lymphoma therapy[J]. Chinese Chemical Letters, 2024, 35(12): 109658.
[29] ZUO S, SONG J, ZHANG J, et, al. Nano-immunotherapy for each stage of cancer cellular immunity: which, why, and what?[J]. Theranostics, 2021, 11(15): 7471-7487.
[30] XIN Y, HUANG M, GUO W W, et, al. Nano-based delivery of RNAi in cancer therapy[J]. Molecular Cancer, 2017, 16(1): 134.
[31] YANG Y, GUO J, HUANG L. Tackling TAMs for Cancer Immunotherapy: It's Nano Time[J]. Trends in Pharmacological Sciences, 2020, 41(10): 701-714.
[32] ZHONG R, TALEBIAN S, MENDES B B, et, al. Hydrogels for RNA delivery[J]. Nature Materials, 2023, 22(7): 818-831.
[33] SHEN W, PEI P, ZHANG C, et, al. A Polymeric Hydrogel to Eliminate Programmed Death-Ligand 1 for Enhanced Tumor Radio-Immunotherapy[J]. ACS nano, 2023, 17(23): 23998-24011.
[34] WU Y, CHANG X, YANG G, et, al. A Physiologically Responsive Nanocomposite Hydrogel for Treatment of Head and Neck Squamous Cell Carcinoma via Proteolysis-Targeting Chimeras Enhanced Immunotherapy[J]. Advanced Materials (Deerfield Beach, Fla.), 2023, 35(12): e2210787.
[35] LUO Y, LI J, HU Y, et, al. Injectable thermo-responsive nano-hydrogel loading triptolide for the anti-breast cancer enhancement via localized treatment based on "two strikes" effects[J]. Acta Pharmaceutica Sinica. B, 2020, 10(11): 2227-2245.
[36] ZHU X, LI J, NING H, et, al. α-Mangostin Induces Apoptosis and Inhibits Metastasis of Breast Cancer Cells via Regulating RXRα-AKT Signaling Pathway[J]. Frontiers in Pharmacology, 2021, 12[2024-10-31].
[37] DAS T, ANAND U, PANDEY S K, et, al. Therapeutic strategies to overcome taxane resistance in cancer[J]. Drug Resistance Updates: Reviews and Commentaries in Antimicrobial and Anticancer Chemotherapy, 2021, 55: 100754.
[38] JIA C, LIU Q, ZHANG M, et, al. Engineering Nano-Pills to Inhibit Ovarian Cancer Proliferation and Migration through a Combination of Chemical/Nucleic

Acid Therapy[J]. Small (Weinheim an Der Bergstrasse, Germany), 2024: e2408095.

[39] YOU Y, XU J, LIU Y, et, al. Tailored Apoptotic Vesicle Delivery Platform for Inflammatory Regulation and Tissue Repair to Ameliorate Ischemic Stroke[J]. ACS nano, 2023, 17(9): 8646-8662.

[40] MONTALTO F I, DE AMICIS F. Cyclin D1 in Cancer: A Molecular Connection for Cell Cycle Control, Adhesion and Invasion in Tumor and Stroma[J]. Cells, 2020, 9(12): 2648.

- **Figures**

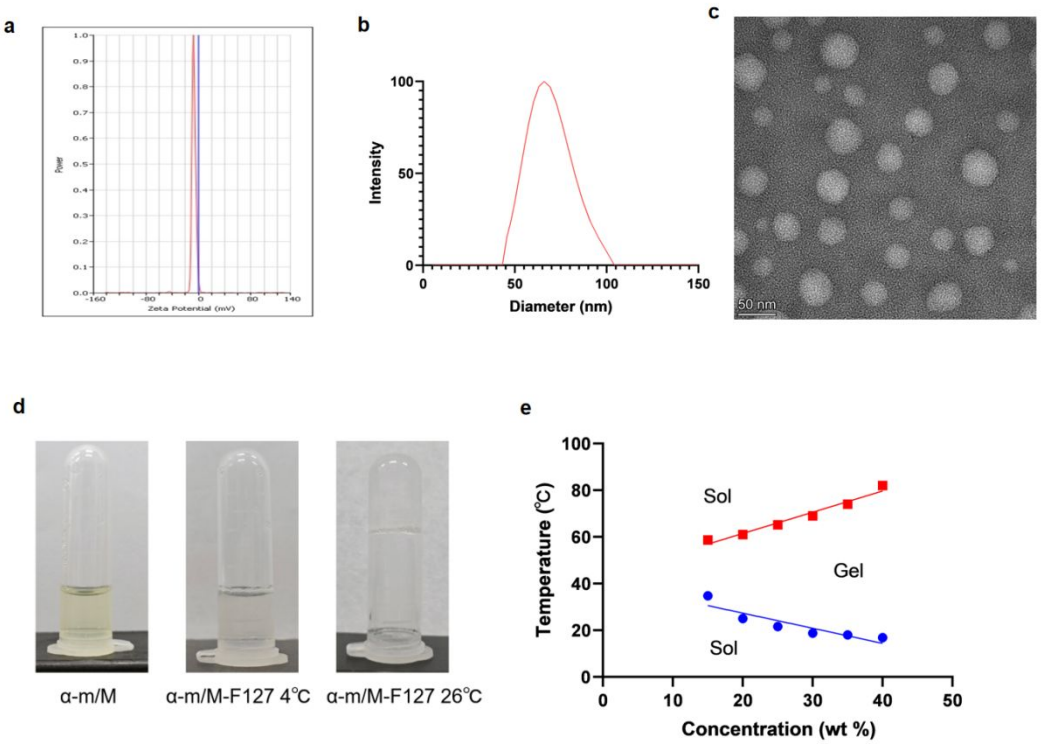

Figure 1. Characterization of alpha-mangostin nanoformulations. **a.** The zeta potential graph of the alpha-mangostin nanoformulation. **b.** The particle size distribution graph of the alpha-mangostin nanoformulation. **c.** The transmission electron microscopy (TEM) image of the alpha-mangostin nanoformulation. **d.** The schematic diagram of the alpha-mangostin nanoformulation. **e.** The process of F127 forming a thermosensitive gel.

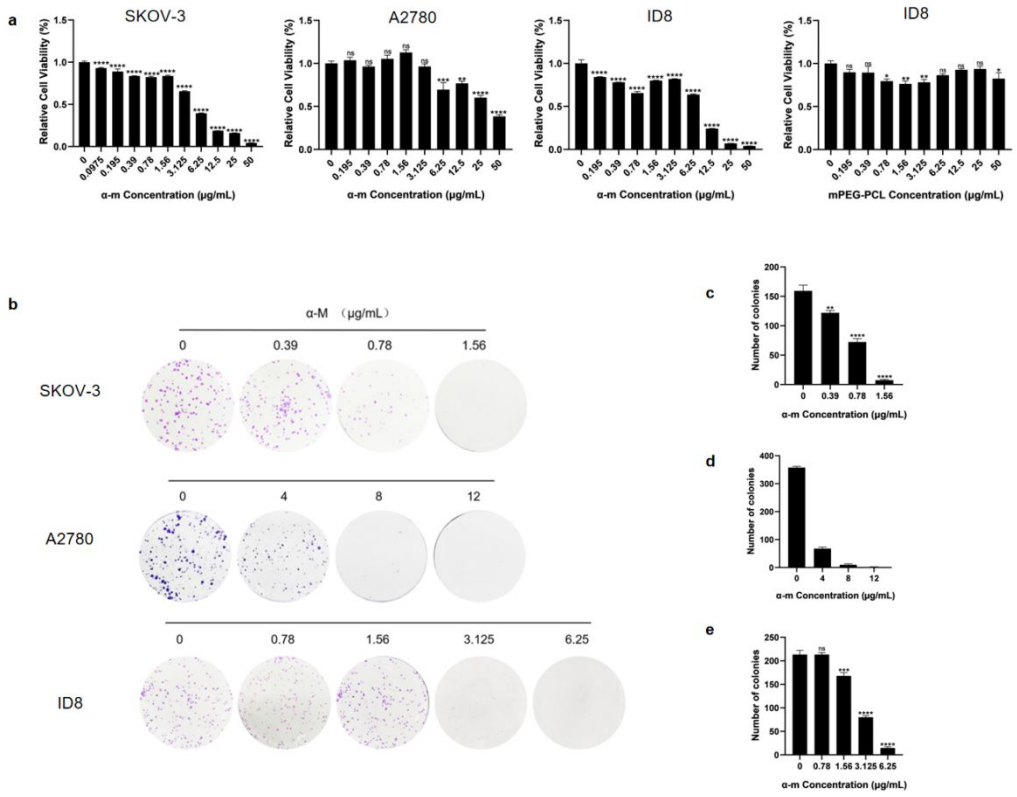

Figure 2. Cell viability studies and proliferation inhibition effects of alpha-mangostin. a. After co-incubating different concentrations of alpha-mangostin nanoformulations with ovarian cancer cells SKOV-3, A2780, and ID8 for 24 or 48 hours in vitro, cell viability was assessed using the MTT assay kit (n=3). After co-incubating ovarian cancer cells ID8 with various concentrations of mPEG-PCL for 24 hours in vitro, cell viability was assessed using the MTT assay kit (n=3). **b.** Two weeks after co-incubating different concentrations of alpha-mangostin nanoformulations with ovarian cancer cells SKOV-3, A2780, and ID8 in vitro, colony formation of cells in different treatment groups (n=3). **c.** Count of clones formed by SKOV-3 cells after treatment with different concentrations of alpha-mangostin nanoformulations for two weeks. **d.** Count of clones formed by A2780 cells after treatment with different concentrations of alpha-mangostin nanoformulations for two weeks. **e.** Count of clones formed by ID8 cells after treatment with different concentrations of alpha-mangostin nanoformulations for two weeks.

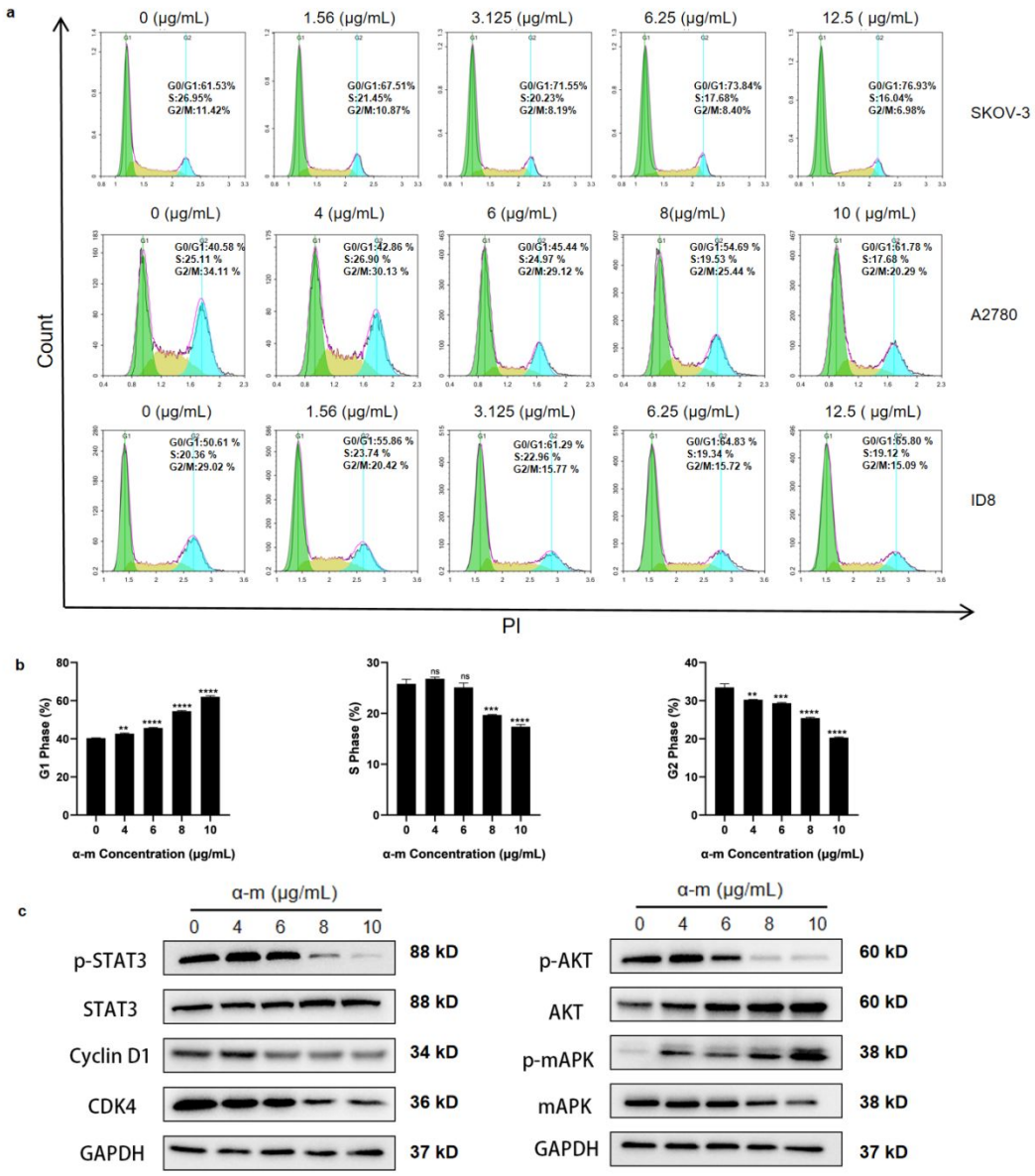

Figure 3. The cell cycle arrest effect of alpha-mangostin. a. Determination of the cell cycle of ovarian cancer cell lines SKOV-3, A2780, and ID8 in vitro using alpha-mangostin nanoformulations. **b.** The percentage of A2780 cells in the G_1, S, and G_2 phases of the cell cycle after treatment with alpha-mangostin nanoformulations. **c.** Expression of proliferation and cell cycle-related proteins in ovarian cancer A2780 cells after treatment with various concentrations of alpha-mangostin nanoformulations for 48 hours (n=3).

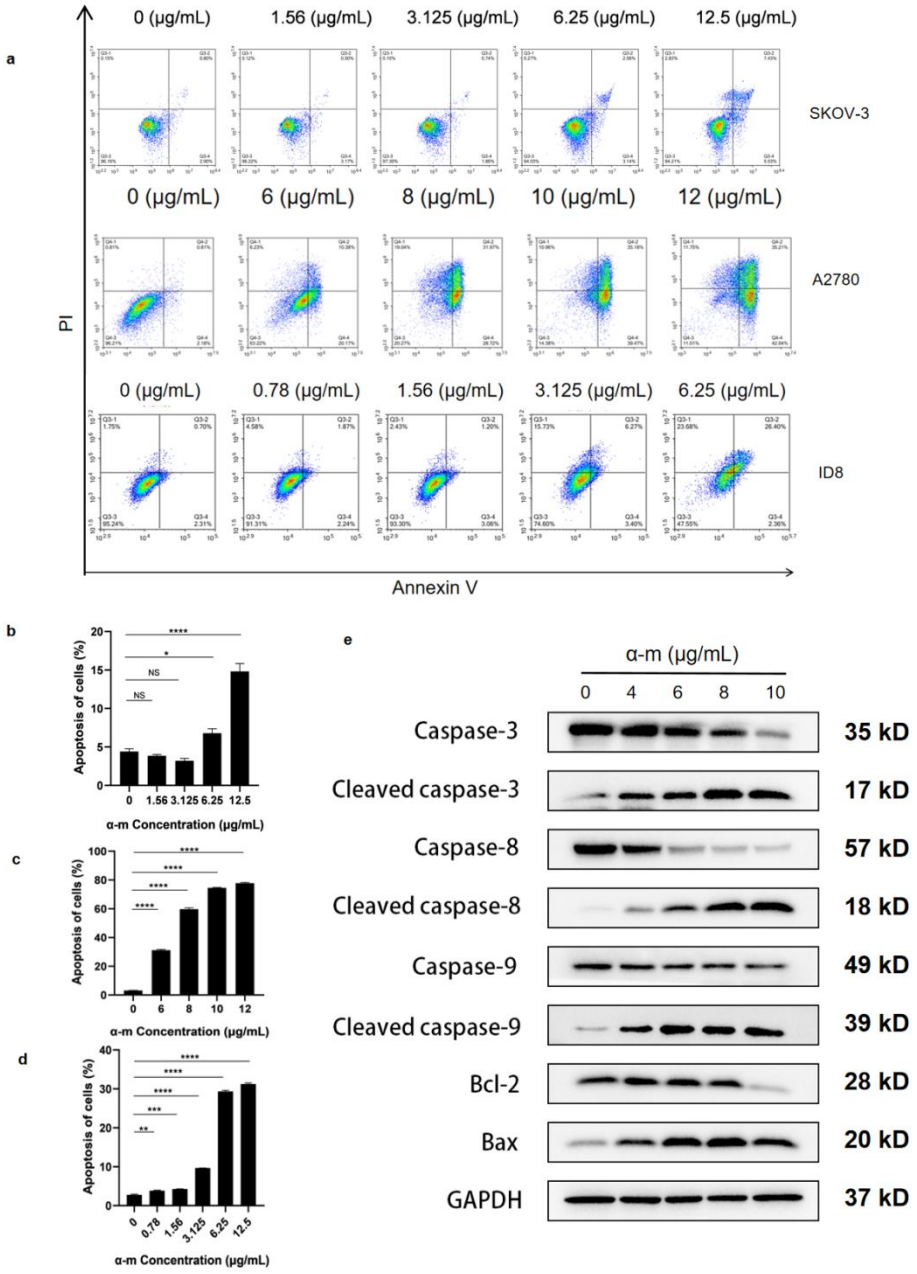

Figure 4. Determination of the apoptotic effect of alpha-mangostin. **a.** Apoptosis assay of alpha-mangostin nanoformulations against ovarian cancer cell lines SKOV-3, A2780, and ID8 in vitro (n=3). **b.** Apoptosis ratio of ovarian cancer SKOV-3 cells after treatment with various concentrations of alpha-mangostin nanoformulations for 48 hours. **c.** Apoptosis ratio of ovarian cancer A2780 cells after treatment with various concentrations of alpha-mangostin nanoformulations for 48 hours. **d.** Apoptosis ratio of ovarian cancer ID8 cells after treatment with various concentrations of alpha-

Academic Press

mangostin nanoformulations for 48 hours. **e.** Expression of apoptosis-related proteins in ovarian cancer A2780 cells after treatment with various concentrations of alpha-mangostin nanoformulations for 48 hours (n=3).

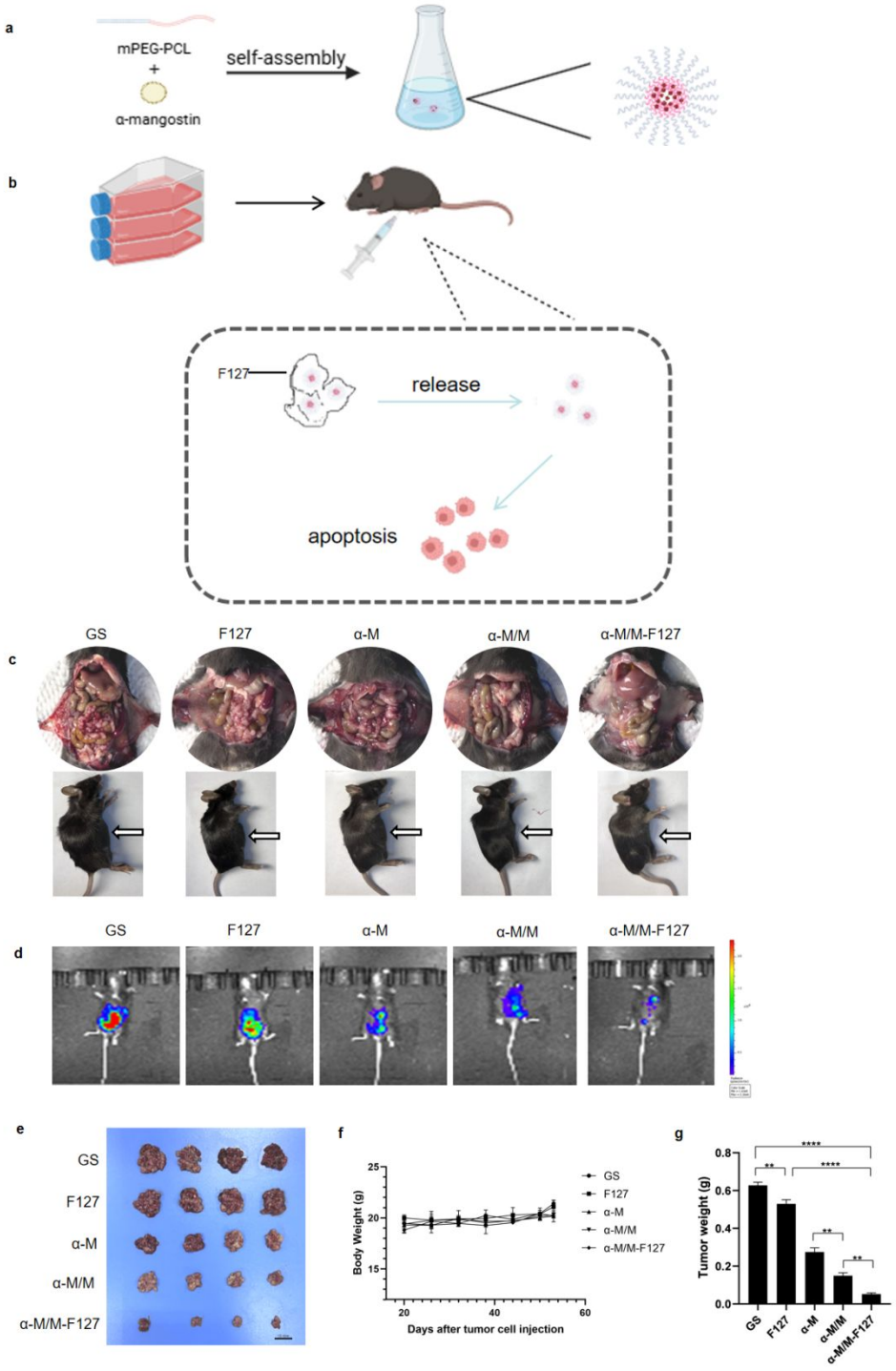

Figure 5. Schematic diagram of alpha-mangostin nanoformulation preparation and induction of tumor cell apoptosis, and the antitumor activity of F127 hydrogel-

Academic Press

encapsulated alpha-mangostin nanoformulations in an ovarian cancer peritoneal dissemination model. **a.** Schematic diagram of the preparation of alpha-mangostin nanoformulations. **b.** Schematic diagram of the inoculation of ID8-luc ovarian cancer peritoneal animal model and the in vivo action of the drug. **c.** Schematic diagram of the preparation of alpha-mangostin nanoformulations. **d.** In vivo imaging images of tumor-bearing mice treated with different groups. **e.** Images of tumors from different groups. **f.** Graph of body weight changes in tumor-bearing mice. **g.** Tumor weight (n=4).

Academic Press

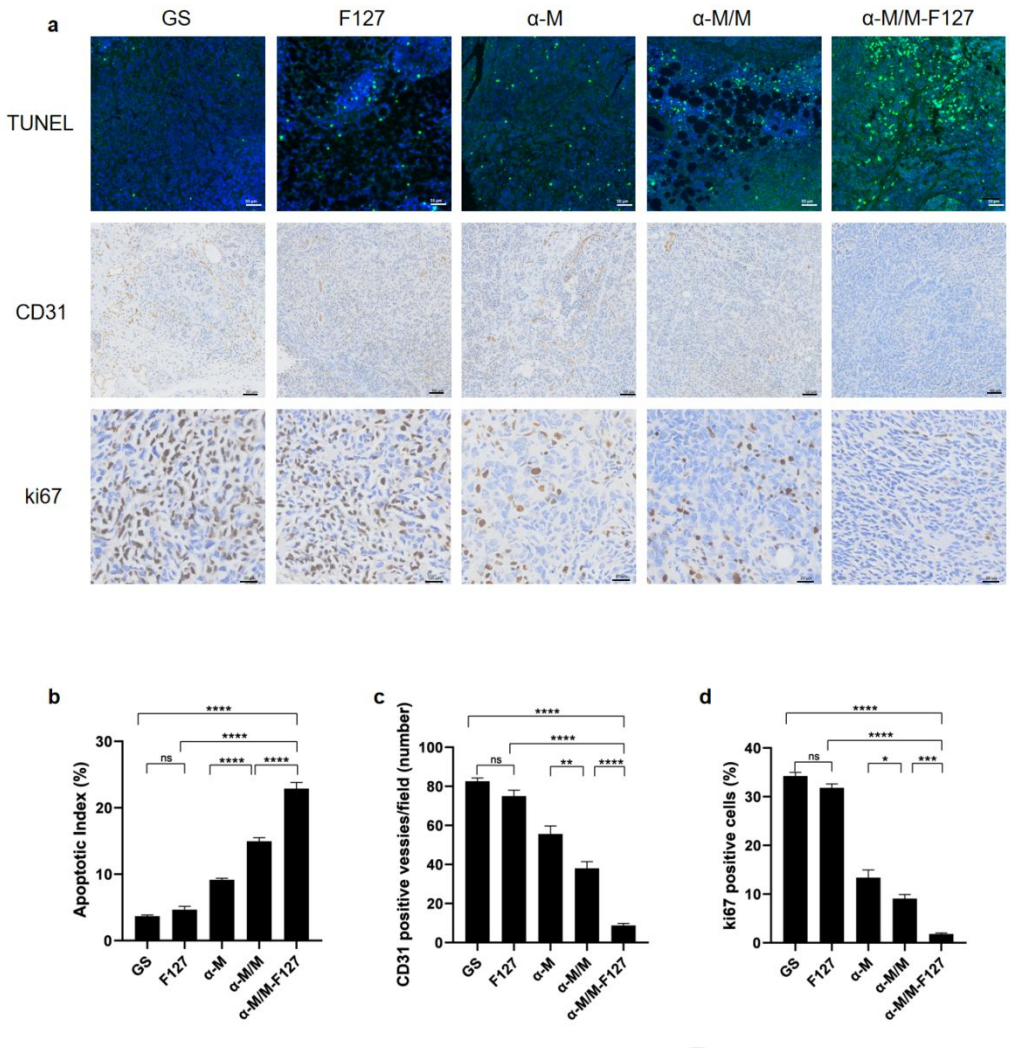

Figure 6. In vivo determination of cell apoptosis, angiogenesis, and proliferation. **a.** TUNEL, CD31, and Ki67 immunohistochemical staining in the mouse ID8 ovarian cancer model to assess the effects of different drug treatments on tumor cell apoptosis, angiogenesis, and in vivo proliferation. **b.** Average percentage of TUNEL-positive cells (n=5). **c.** Average number of positive blood vessels (n=5). **d.** Average percentage of Ki67-positive cells (n=5).

Academic Press

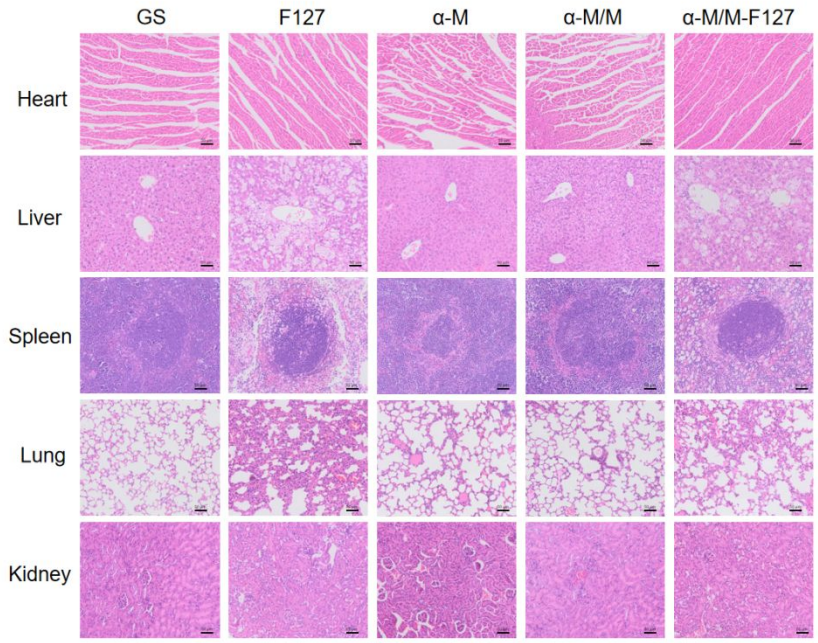

Figure 7. Representative H&E staining images of hearts, livers, spleens, kidneys, and lungs from different groups at the end of the treatment period, (n=5).

Academic Press

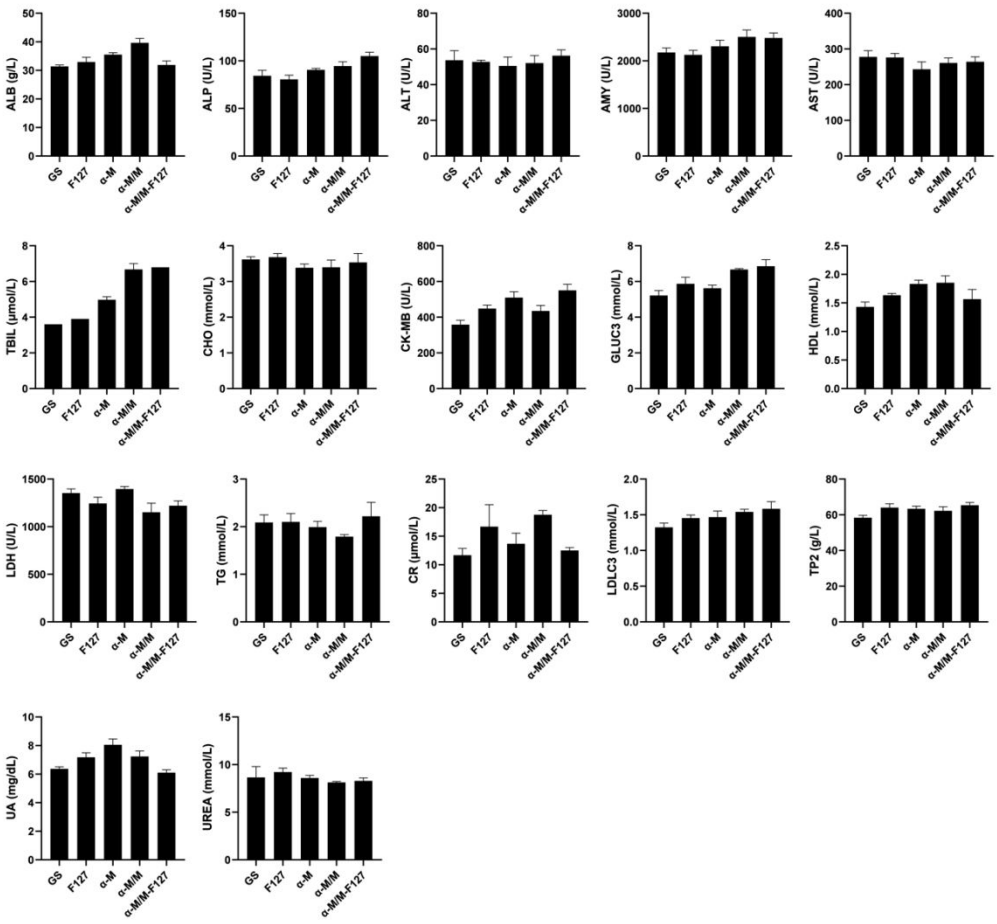

Figure 8. Analysis of serum biochemical markers from different groups, (n=5).

Academic Press

- **Biographies**

Xia Liu graduated from Hainan University in 2023 with a bachelor's degree and is currently a master's student at the National Key Laboratory of Biotherapy, Sichuan University. She has joined Professor Xiang Gao's research group, focusing on research areas such as anticancer drugs and nanomaterials.